https://doi.org/10.1016/j.fuel.2017.03.003

Syngas production from CO_2/CH_4 rich combustion in a porous media burner: Experimental characterization and elementary reaction model

Hongyu Zeng [a,b], Yuqing Wang [a], Yixiang Shi [a,*], Meng Ni [b,*], Ningsheng Cai [a]

[a] Key Laboratory for Thermal Science and Power Engineering of Ministry of Education, Department of Thermal Engineering, Tsinghua University, Beijing 100084, China
[b] Building Energy Research Group, Department of Building and Real Estate, The Hong Kong Polytechnic University, Hung Hom, Kowloon, Hong Kong, China

Abstract

Methane and carbon dioxide are two major components in many biomass-derived gases such as landfill gas and biogas, which are renewable and have potential fuel cell applications. Syngas production from non-catalytic and fuel-rich combustion using a two-layer porous media burner was studied experimentally and numerically with a range of CO_2 content in the CH_4 fuel. With an air flow rate of 5 L/min, an equivalence ratio of 1.5 and a mole ratio of CO_2/CH_4 of 1, the reforming efficiency was found to be 45.3%, larger than that (39.1%) without CO_2 in the feed at the same air flow rate and equivalence ratio. A two-dimensional model with an elementary reaction mechanism was developed to study the influence of carbon dioxide on the reforming characteristics. The model is validated by the experimental results with good agreement. The simulation results clearly showed that the reaction process along the burner could be divided into a preheating zone, a CO_2-consuming zone and a CO_2-generating zone according to the net reaction rate of CO_2.

Keywords

Carbon dioxide
Rich combustion
Porous media
Reaction mechanism

1. Introduction

Conventional fossil fuels will not be able to meet the increasing energy demand for a long time but also produce serious pollution. Biomass-derived gas is abundant, cheap, and renewable energy that contains a mole fraction of 50 ~ 80% methane (CH_4) and 20 ~ 50% carbon dioxide (CO_2) [1]. Syngas production from biomass-derived gas for fuel cells [2], [3] is a potential way to utilize two greenhouse gases [4], [5], [6], especially for distributed combined heat and power (CHP) systems with distributed biogas.

For syngas production from biomass-derived gases, many studies regarding dry reforming and autothermal reforming of CH_4 and CO_2 have been conducted, especially on the development of different catalysts [7], [8], [9]. Due to the high carbon content of CH_4 and CO_2, carbon deposition is usually a serious problem for the methane reforming processes, as the deposited solid carbon can block the reaction sites on the catalyst surface. To solve this problem, adding a certain amount of oxygen into the gas mixture was proposed by some researchers to reduce the carbon deposition. However, the injected oxygen favors strong oxidation reaction in the upstream zone which substantially increases the local temperature and leads to the sintering of catalysts [10], [11]. In order to solve the problem of coking, sintering and catalyst deactivation, an alternative method is to develop catalyst-free process. The fuel-rich combustion, a non-catalytic partial oxidation reforming method without any extra heating, could be a feasible method to utilize biomass-derived gas for syngas production.

A large amount of CO_2 in the fuel gas decreases the rich flammability limit of fuel in free flames. Some solutions were proposed to expand the flammability, such as preheating the inlet gases, boosting the pressure, or using pure oxygen to replace the air. However, these methods increase the energy consumption during the reforming process. Syngas production from the fuel-rich combustion of methane [12], heptane [13], ethanol [14], etc. in porous media combustors has been studied and good performance has been achieved. During the combustion in a porous media burner, the heat of combustion could be easily transferred upstream to preheat the premixed reaction gases. In this way, the heat of the combustion of the exhaust gas can be recovered effectively, thus expanding the flammability limit and improving the reforming efficiency. Therefore, using a porous media burner for the rich combustion of biomass-derived gas is probably a practical process.

For the flame in porous media burner, filtration combustion and stability combustion are usually applied [15]. To ensure stable operation, stability combustion in a two-layer porous media burner is considered a safe and feasible method in terms of material requirements and reliability [16]. Pedersen-Mjaanes et al. used a two-layer porous media burner to stabilize the fuel-rich flame of methane. The reforming efficiency reached 45% when the equivalence ratio was 1.85 [17]. Wang et al. used a two-layer porous media burner with a micro-tubular SOFC for a flame fuel cell. Using methane as the fuel, the power of a single cell reached 1.5 W at 0.7 V, which was a good demonstration of porous media burner as a non-catalytic fuel processor for an SOFC [18]. Although there have been some experimental and numerical studies for the fuel-rich combustion of methane in a two-layer porous media burner [19], [20], the reaction characteristics of the CO_2/CH_4 mixture in the burner and the effect of different

amount of CO_2 in the fuel is not clear so far. The reaction mechanisms and the heat transfer mechanisms have not been studied before for the injection of CO_2.

In this study, a two-layer porous media burner was applied to experimentally produce syngas from biomass-derived gas with different amount of CO_2. Based on the experimental setup, an elementary reaction model was developed, considering the mass-transport and heat-transport in the porous medium. The computed temperature distributions and the gas compositions at the outlet were compared with the experimental results and good agreement was obtained. Parametric simulations were conducted to understand the gas composition variation along the burner and the effect of CO_2 addition on the combustion characteristics.

2. Experimental and modeling

2.1. Experimental setup

The schematic diagram of the whole experimental system was shown in Fig. 1. Three gas feeds of air, CO_2, CH_4 were regulated into the premixed chamber from the gas tank through a pressure-reducing valve, a mass flow controller and a check valve, respectively. In the premixed chamber, the inlet gases were well mixed and then passed into the anti-flashback chamber, which was filled with 1–2 mm quartz sand. A fine stainless steel mesh was placed on the anti-flashback chamber to disperse the extra heat, further preventing flashback. After that, the inlet premixed gases flowed through two layers of porous media. The shell of the porous media burner was a stainless tube with an external diameter of 60 mm, an internal diameter of 54 mm and a height of 200 mm. Formed aluminum silicate insulation materials with an internal diameter of 30 mm were placed into the stainless tube to protect the tube from high temperature, which means the effective diameter of the flow path was 30 mm. The outside of the stainless burner was insulated with 65 mm of quartz fiber to reduce the heat leak. Al_2O_3 pellets of different diameters were used as the porous media materials. The porous media burner was filled with a 20 mm depth of 2–3 mm pellets on the upstream end, and filled with a 60 mm depth of 7.5 mm in diameter on the downstream end. All the pellets were solid spheres of α-Al_2O_3, with no activity. They did not change after the experiments. The temperature profile along the axis of the burner was measured by 7 S-type thermocouples labeled from T1 to T7, with a diameter of 3 mm. The thermocouples were spaced uniformly at 10 mm intervals from upstream to downstream, as shown in Fig. 1. With a micro-pump, the exhaust gases were pumped into a drying tube and then were sampled to a gas sample bag, after the flame was stabilized. A gas chromatograph (GC) was used to measure the concentration of H_2, CO, CO_2, and CH_4 in the exhaust gases.

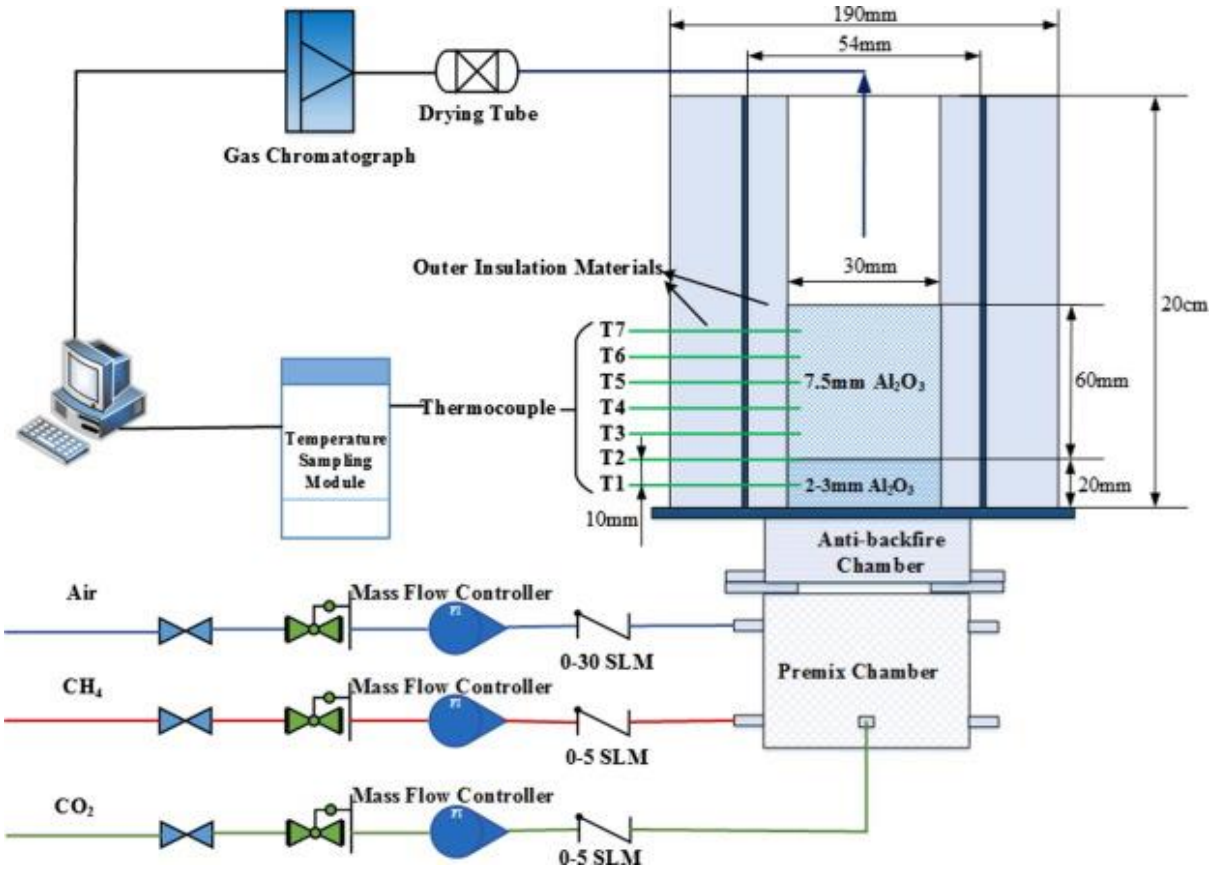

Fig. 1. The experimental system of CO_2/CH_4 rich combustion in a porous media burner.

2.2. Experimental procedure

Spark ignition was used to start the procedure at the exit of the combustion chamber, which was open to the outside atmosphere. When using fuel-rich operating conditions in the ignition, the flame will stay on the surface and cannot propagate into the porous media and upstream. Therefore, fuel-lean operating conditions were usually adopted to ignite the burner. After ignition, the flame remained on the surface of the downstream porous media for a while to preheat the downstream pellets. Several minutes later, the flame gradually propagated into the internal pellets and preheated the pellets. When the upstream pellets reached 600 °C, in other words, when the thermocouple T1 reached 600 °C, the fuel-lean operating conditions were changed to the fuel-rich conditions to be studied. When all the temperatures monitored by the thermocouples did not change for 20 min, the flame was considered to be stable. In this case, the whole system reached thermal equilibrium. After that, the outlet products were sampled and then analyzed by GC. All the measured temperatures were corrected for radiation effects [21].

2.3. Parameter definitions

The equivalence ratio ϕ is defined as

$$\phi = \frac{n_{fuel}/n_{air}}{n^s_{fuel}/n^s_{air}} = \frac{\dot{V}_{fuel}/\dot{V}_{air}}{\dot{V}^s_{fuel}/\dot{V}^s_{air}} \quad (1)$$

where n_{fuel} and n_{air} are the mole numbers of the fuel (which is the mixture of CO_2 and CH_4) and air, respectively. $\dot{V}_{fuel}$ and $\dot{V}_{air}$ are the volumetric flow rates of the fuel and air, respectively, which were regulated by mass flow controllers. n_{fuels}, n_{airs}, $\dot{V}_{fuels}$ and $\dot{V}_{airs}$ are those parameters in stoichiometric conditions.

The ratio CO_2/CH_4 is defined as

$$CO_2/CH_4 = \frac{\dot{V}_{CO_2}}{\dot{V}_{CH_4}} \quad (2)$$

where $\dot{V}_{CO2}$ and $\dot{V}_{CH4}$ are the volumetric flow rates of CO_2 and CH_4. This ratio means the proportion of CO_2 and CH_4 in the fuel.

The reforming efficiency is defined as

$$\eta = \frac{chemical\ energy\ of\ H_2\ and\ CO}{input\ chemical\ energy\ of\ initial\ fuel} = \frac{Y_{H_2,out}LHV_{H_2} + Y_{CO,out}LHV_{CO}}{Y_{fuel,in}LHV_{fuel}} \quad (3)$$

where Y is the mass fraction, LHV_{H2}=120.1MJ/kg, LHV_{CO}=10125.1kJ/kg, in this case, Y_{fuelin} $LHV_{fuel}=Y_{CH4,in}LHV_{CH4}$, and LHV_{CH4}=50184.5kJ/kg.

2.4. Model assumptions and geometry

A model was developed to simulate the experiments, considering the pressure loss of the gases flowing through the porous media, solid radiation inside the porous medium, local non-equilibrium convective heat-transfer between gas and solid phase, and elementary reactions.

The following assumptions were applied in the model:

(1) 2D, axis symmetry, steady state;
(2) Gases were considered as incompressible ideal gases;
(3) Porous media were homogeneous and isotropic, and catalysis from porous media was neglected;
(4) Gas radiation was neglected;
(5) Gas flow in the porous media was regarded as laminar flow.

The computational domain for the porous zone, shown in Fig. 2, is 80 mm long and consists of two layers of Al_2O_3 pellets with different diameters. In view of both computational accuracy

and calculating speed of the computer, the grid independence was verified. For the chemical reactions mainly occurring in the upstream layer or near the interface, the mesh of the first 30 mm from inlet was densified. The computational domain was discretized into 950 cells in the upstream layer and 1653 cells in the downstream.

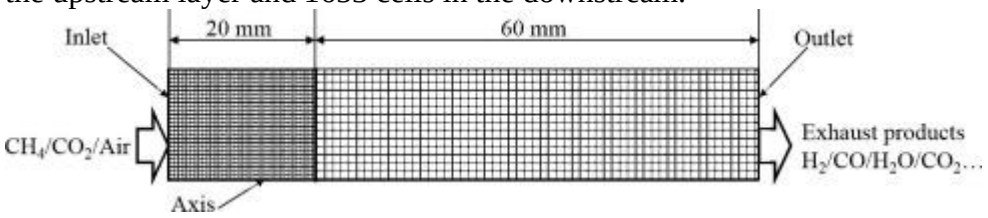

Fig. 2. Computational domain and boundaries of the two-layer porous media burner.

2.5. Governing equations and boundary conditions

Governing equations for mass, momentum, gas energy, solid energy, and gas species were solved:

Continuity equation:

$$\vec{\nabla}\cdot(\varepsilon\rho_g\vec{v})=0 \tag{4}$$

where ε is the porosity of the porous media, ρ_g is the gas density, $\vec{v}$ is the actual velocity of the gas flow in the porous media, namely, physical velocity. The porosity was calculated as ε=0.375+0.34d/D [22], where d is the particle diameter and D is the inner diameter of reactor, 30 mm in this study.

Momentum equation:(5)

$$\vec{\nabla}\cdot(\varepsilon\rho_g\vec{v}\cdot\vec{v})=-\nabla(\varepsilon p)+\vec{\nabla}\cdot(\varepsilon\bar{\bar{\tau}})+\vec{F} \tag{5}$$

where τ is the viscosity stress tensor, and F is the pressure loss term given by the Ergun equation:

$$\vec{F}=-150\frac{(1-\varepsilon)^2\mu_g}{d^2\varepsilon^2}\vec{v}-1.75\frac{\rho_g(1-\varepsilon)|\vec{v}|}{d\varepsilon}\vec{v} \tag{6}$$

Gas energy equation:

$$\vec{\nabla}(\varepsilon\vec{v}\cdot\rho_g C_g T_g)=\vec{\nabla}\cdot(\varepsilon\lambda_g\nabla T_g)+\varepsilon\sum_{i=1}^{N_{r,g}}\omega_i h_i W_i-h_v(T_g-T_s) \tag{7}$$

where C_g is the specific heat of the gas mixture; T_g is the gas temperature; λ_g is the thermal conductivity of the gas mixture; $\sum_{i=1}^{N_{r,g}}\omega_i h_i W_i$ is the gas-phase chemical reaction heats; and $h_v(T_g-T_s)$ is the heat transfer between gas and solid, where hv is the volumetric convective heat-transfer coefficient and was calculated by $h_v=6\varepsilon Nu_v\lambda_g/d^2$. Here, Nu_v is the Nusselt

number and was given by the regression formula from Wakao and Kaguei: $Nu_v=2+1.1Pr^{1/3}Re^{0.6}$, where Pr is the Prandtl number and Re is the Reynolds number.

Solid energy equation:

$$\vec{\nabla}\cdot(\lambda_{eff-s}\nabla T)+h_v(T_g-T_s)=0 \quad (8)$$

where λ_{eff-s} is the effective thermal conductivity of the porous media and was given by $\lambda_{eff-s}=(1-\varepsilon)\lambda_s+\lambda_{rad}$. λ_{rad} is the radiative conductivity of alumina pellets and is described by the Rosseland approximation, and can be calculated as $\lambda_{rad}=(32\varepsilon\sigma d/9(1-\varepsilon))Ts^3$, where $\sigma=5.67\times10-8Js^{-1}m^{-2}K^{-4}$ is the Stefan-Boltzmann number.

Species transport equation:

$$\vec{\nabla}\cdot(\varepsilon\rho_g\vec{v}Y_i)=\vec{\nabla}\cdot(\varepsilon\rho_g Y_i V_i)+\varepsilon\omega_i W_i \quad (9)$$

where V_i is the diffusion velocity for species i.

The ideal gas equation of state is also used in the model, which was defined as

$$p=\rho_g RT_g \quad (10)$$

The following boundary conditions were specified in the model:

(1) Side wall: vr=0, T_{wall_out}=300K, thickness_wall=80mm;

(2) Inlet: $v_x=v_{in}$, $v_r=0$, $Y_i=Y_{i,in}$, T_g=300K, $\lambda_{eff-s}\nabla Ts=-\xi\sigma(T_{s,in}^4-T_0^4)$; (where the emissivity ξ=0.8)

(3) Outlet: $\frac{\partial v_x}{\partial x}=\frac{\partial Y_i}{\partial x}=\frac{\partial T_g}{\partial x}=\frac{\partial T_s}{\partial x}=0,\quad \lambda_{eff-s}\nabla T_s=-\xi\sigma(T_{s,out}^4-T_0^4)$ (where the emissivity ξ=0.8)

The N. Peters Reduced Mechanism [23], including 17 gas-phase species and 58 elementary homogeneous reactions, was adopted. The detailed mechanisms and reaction rates of N. Peter reduced mechanism were shown in Table 1. The model was solved with ANSYS Fluent and the reaction mechanism was imported from CHEMKIN. A high temperature of 1500 K was patched for the downstream zone initially for ignition.

Table 1. The detailed mechanisms and reaction rates of N. Peter reduced mechanism.

R*x*	**Reaction**	**A[a]**	**β**	**Ea**
Homogeneous reactions				
1	$CH_3 + H + M = CH_4 + M$	8.00×10^{20}	-3	0
2	$CH_4 + O_2 = CH_3 + HO_2$	7.90×10^{10}	0	2.34×10^8
3	$CH_4 + H = CH_3 + H_2$	22	3	3.66×10^7
4	$CH_4 + O = CH_3 + OH$	1.60×10^3	2.36	3.10×10^7
5	$CH_4 + OH = CH_3 + H_2O$	1.60×10^3	2.10	1.03×10^7
6	$CH_3 + OCH_2O + H$	6.80×10^{10}	0	0

R*x*	**Reaction**	**A[a]**	**β**	**Ea**
7	$CH_3 + OH = CH_2O + H_2$	1.00×10^{9}	0	0
8	$CH_3 + OH = CH_2 + H_2O$	1.50×10^{10}	0	2.09×10^{7}
9	$CH_3 + H = CH_2 + H_2$	9.00×10^{10}	0	6.32×10^{7}
10	$CH_2 + H = CH + H_2$	1.40×10^{16}	-2	0
11	$CH_2 + OH = CH_2O + H$	2.50×10^{10}	0	0
12	$CH_2 + OH = CH + H_2O$	4.50×10^{10}	0	1.26×10^{7}
13	$CH + O_2 = HCO + O$	3.30×10^{10}	0	0
14	$CH + O = CO + H$	5.70×10^{10}	0	0
15	$CH + OH = HCO + H$	3.00×10^{10}	0	0
16	$CH + CO_2 = HCO + CO$	3.40×10^{9}	0	2.89×10^{6}
17	$CH_2 + CO_2 = CH_2O + CO$	1.10×10^{8}	0	4.18×10^{6}
18	$CH_2 + O = CO + H + H$	3.00×10^{10}	0	0
19	$CH_2 + O = CO + H_2$	5.00×10^{10}	0	0
20	$CH_2 + O_2 = CO_2 + H + H$	1.60×10^{9}	0	4.18×10^{6}
21	$CH_2 + O_2 = CH_2O + O$	5.00×10^{10}	0	3.77×10^{7}
22	$CH_2 + O_2 = CO_2 + H_2$	6.90×10^{8}	0	2.09×10^{6}
23	$CH_2 + O_2 = CO + H_2O$	1.90×10^{7}	0	-4.18×10^{6}
24	$CH_2 + O_2 = CO + OH + H$	8.60×10^{7}	0	-2.09×10^{6}
25	$CH_2 + O_2 = HCO + OH$	4.30×10^{7}	0	-2.09×10^{6}
26	$CH_2O + OH = HCO + H_2O$	3.43×10^{6}	1.18	-1.87×10^{6}
27	$CH_2O + H = HCO + H_2$	2.19×10^{5}	1.77	1.26×10^{7}
28	$CH_2O + M = HCO + H + M$	3.31×10^{13}	0	3.39×10^{8}
29	$CH_2O + O = HCO + OH$	1.81×10^{10}	0	1.29×10^{7}
30	$HCO + OH = CO + H_2O$	5.00×10^{9}	0	0
31	$HCO + M = H + CO + M$	1.60×10^{11}	0	6.15×10^{7}
32	$HCO + H = CO + H_2$	4.00×10^{10}	0	0
33	$HCO + O = CO_2 + H$	1.00×10^{10}	0	0
34	$HCO + O_2 = HO_2 + CO$	3.30×10^{10}	-0.40	0
35	$CO + O + M = CO_2 + M$	3.20×10^{7}	0	-1.76×10^{7}
36	$CO + OH = CO_2 + H$	1.51×10^{4}	1.30	-3.17×10^{6}
37	$CO + O_2 = CO_2 + O$	1.60×10^{10}	0	1.72×10^{8}

R*x*	**Reaction**	**A[a]**	**β**	**Ea**
38	$HO_2 + CO=O_2 + OH$	5.80×10^{10}	0	9.60×10^{7}
39	$H_2 + O_2=2OH$	1.70×10^{10}	0	2.00×10^{8}
40	$OH + H_2=H_2O + H$	1.17×10^{6}	1.30	1.52×10^{7}
41	$H + O_2=OH + O$	5.13×10^{13}	−0.82	6.91×10^{7}
42	$O + H_2=OH + H$	1.80×10^{7}	1	3.69×10^{7}
43	$H + O_2 + M=HO_2 + M$	3.61×10^{11}	−0.72	0
44	$OH + HO_2=H_2O + O_2$	7.50×10^{9}	0	0
45	$H + HO_2=2OH$	1.40×10^{11}	0	4.49×10^{6}
46	$O + HO_2=O_2 + OH$	1.40×10^{10}	0	4.49×10^{6}
47	$2OH=O + H_2O$	6.00×10^{5}	1.30	0
48	$H + H + M=H_2 + M$	1.00×10^{12}	−1	0
49	$H + H + H_2=H_2 + H_2$	9.20×10^{10}	−0.60	0
50	$H + H + H_2O=H_2 + H_2O$	6.00×10^{13}	−1.25	0
51	$H + H + CO_2=H_2 + CO_2$	5.49×10^{14}	−2	0
52	$H + OH + M=H_2O + M$	1.60×10^{16}	−2	0
53	$H + O + M=OH + M$	6.20×10^{10}	−0.6	0
54	$H + HO_2=H_2 + O_2$	1.25×10^{10}	0	0
55	$HO_2 + HO_2=H_2O_2 + O_2$	2.00×10^{9}	0	0
56	$H_2O_2 + M=OH + OH + M$	1.30×10^{14}	0	1.90×10^{8}
57	$H_2O_2 + H=HO_2 + H_2$	1.60×10^{9}	0	1.59×10^{7}
58	$H_2O_2 + OH=H_2O + HO_2$	1.00×10^{10}	0	7.53×10^{6}

a

Arrhenius parameters for the rate constant written in the form: $k=AT^{\beta}exp(-E/RT)$. The units of *A* are given in terms of kmol, m, and s. E is in J/kmol.

3. Results and discussion

In the experiment, the required operating conditions were regulated after the preheating process was finished. With a fixed air flow rate of 5 L/min, the flow rates of CO_2 and CH_4 were changed to adjust the equivalence ratio and the ratio CO_2/CH_4. After the experiment with a number of firing cycles, no carbon deposition was found on the Al_2O_3 pellets.

3.1. Temperature distribution

When the air flow rate was fixed at 5 L/min and the equivalence ratio was 1.5, the experimental and numerical results of the temperature distribution were shown in the Fig. 3 for the ratios of CO_2/CH_4 of 0 and 1. As Fig. 3 shows, the numerical results for the temperature match well with the experimental results, indicating that the model settings and parameters were reasonable. Since it was unknown whether the temperatures measured by the thermocouples were of the gas phase or the solid phase, the numerical model can be a useful tool to estimate both the gas temperature and the solid temperature. From the numerical results, in the upstream zone for flame, the solid temperature was higher than the gas temperature due to the solid heat radiation and conduction from the downstream, thus the inlet premixed fresh gases could be preheated by the porous media. Around the flame surface, due to the large heat release by the combustion reaction, the gas temperature was much higher than the solid temperature. The temperature difference between the solid and gas phases reached several hundred degrees at the position of flame, which indicated that the local-thermal non-equilibrium effect must be considered in the thermal modeling. Therefore, the energy equations for the solid and gas phases should be solved separately, rather than a single general energy equation. In the downstream zone of the flame, the gas temperature was slightly higher than the solid temperature, and part of the heat of combustion of the exhaust gas was recovered by the downstream solid porous media. Due to the excellent heat conduction and radiation performance, the recovered heat could be transferred to the upstream and preheat the inlet premixed gas. Comparing (a) and (b) in Fig. 3, as CO_2 was injected of in the fuel, the flame stabilized at position further downstream, which provided a longer preheating zone.

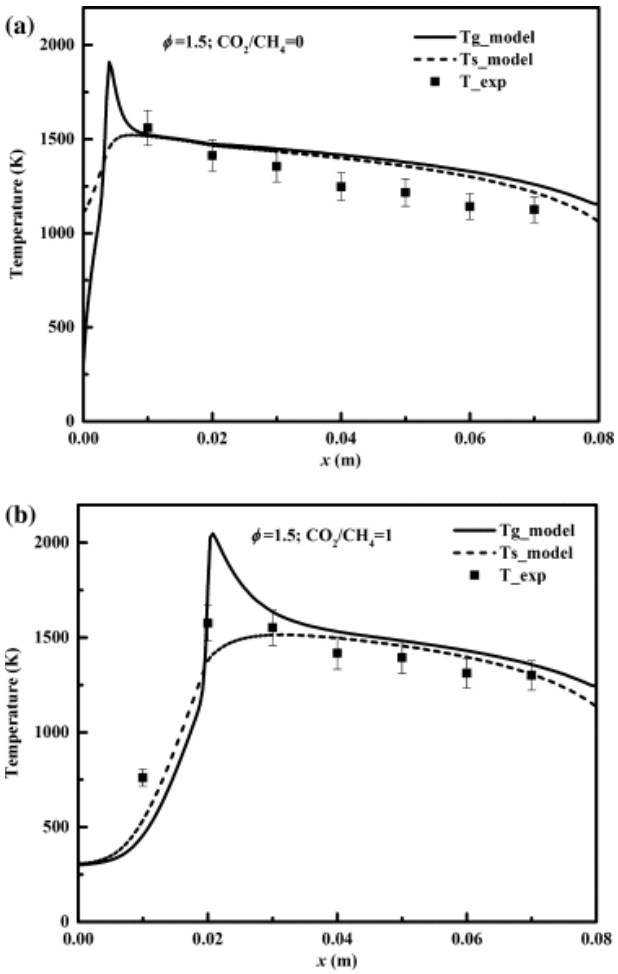

Fig. 3. The temperature profile as the inlet air flow rate was 5 L/min and the equivalence ratio was 1.5, (a)CO_2/CH_4 = 0; (b) CO_2/CH_4 = 1.

3.2. Combustion products and reforming efficiency

The total reaction in the porous media burner can be written as follows:

$$CH_4 + \frac{2}{\phi}(O_2 + 3.76N_2) + xCO_2 \rightarrow (a+x)CO_2 + bCO + cH_2O + dH_2 + \frac{2 \times 3.76}{\phi}N_2$$

where ϕ is the equivalence ratio and x is the ratio of CO_2/CH_4.

When the inlet air flow rate was 5 L/min and the equivalence ratio was 1.5, with different ratios of CO_2/CH_4, the main products in the exhaust gases were shown in Fig. 4, which was calculated to the wet basis. It can be seen that the numerical model predictions of combustion products showed a good agreement with the experimental results. As the CO_2/CH_4 ratio increased, the mole fraction of H_2 decreased and the mole fraction of CO increased at the outlet. The very low mole fraction of CH_4 in the exhaust gases of no more than 1% indicated almost all the methane in the fuel was converted.

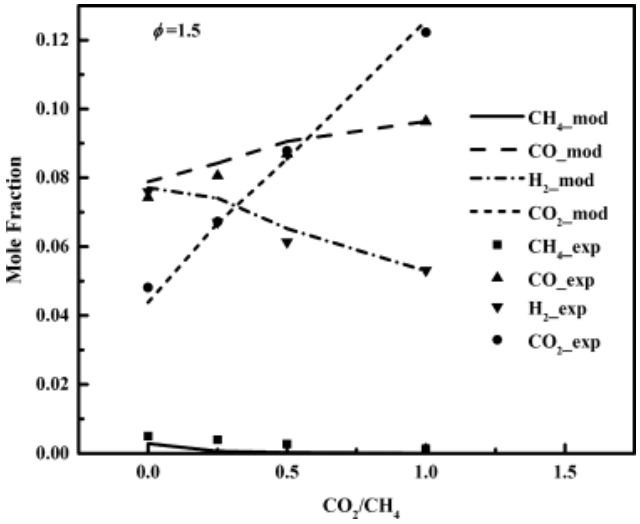

Fig. 4. Flame compositions for various CO_2/CH_4 ratios at inlet air flow rate of 5 L/min and equivalence ratio of 1.5 (wet basis)

Table 2 shows the net emission of CO_2 and the reforming efficiency to syngas for an inlet air flow rate of 5 L/min and an equivalence ratio of 1.5. It is found that the mole fraction and the mass fraction of CO_2 in the outlet increased with increasing inlet CO_2/CH_4 ratio. However, the difference between the outlet mass fraction of CO_2 and the inlet mass fraction of CO_2 was reduced from 8.5% to 1.9% as CO_2/CH_4 increased from 0 to 1. Due to the dilution effect of CO_2 in the fuel, the available energy decreased as the CO_2/CH_4 ratio increased. For a certain absolute available energy, the required total mass flow rate increased, resulting in the increase of CO_2 emission. In order to compare the net CO_2 emission based on the same available energy, the actual net CO_2 emission rate was calculated in Table 2. At an inlet air flow rate of 5 L/min and an equivalence ratio of 1.5, as the inlet CO_2/CH_4 ratio increased from 0 to 1, the absolute available power was all 471 W, the total inlet mass flow rate increased from 0.117 g/s to 0.142 g/s, but the net CO_2 emission rate significantly decreased from 9.87×10^{-3} g/s to 2.67×10^{-3} g/s. It clearly demonstrated that the net emissions for CO_2 could be reduced effectively as CO_2/CH_4 is increased.

Table 2. The net CO_2 emission and the reforming efficiency.

CO_2/CH_4	**ṁt (g/s)[b]**	**Ėt (W)[c]**	$Y_{CO2,out}$	$Y_{CO2,in}$	$Y_{CO2,out}$-$Y_{CO2,in}$	**Net CO_2 emission rate(g/s)**	**η_{exp}**
0	0.117	471	8.5%	0	8.5%	9.87×10^{-3}	39.1%
0.25	0.123	471	11.6%	5.2%	6.3%	7.79×10^{-3}	40.0%
0.5	0.130	471	14.8%	10.0%	4.8%	6.29×10^{-3}	41.8%
1	0.142	471	20.0%	18.1%	1.9%	2.67×10^{-3}	45.3%

[b] Total mass flow rate for various CO_2/CH_4 ratios at inlet air flow rate of 5 L/min and equivalence ratio of 1.5.

[c] Absolute available power.

As the ratio of CO_2/CH_4 increased from 0 to 1, the reforming efficiency of the fuel increased from 39.1% to 45.3%. In the rich combustion process for the mixture of CO_2/CH_4 and air, the chemical energy of methane in the inlet feed could be divided into the chemical energy stored in the syngas and the sensible heat. A large amount of the inlet energy was converted to sensible heat, which was used to maintain the partial oxidation reforming process and then lost along with the exhaust gases. Therefore, to improve the reforming efficiency, the sensible heat loss should be minimized. From Fig. 4, the mole fraction of H_2 decreased while the mole fraction of CO increased with increasing CO_2/CH_4 ratio. The addition of CO_2 in the fuel could promote the inverse water-gas shift (WGS) reaction: $CO + H_2O \rightarrow H_2 + CO_2$, $\Delta H = +41.1$ kJ/mol. The exothermic WGS reaction is an important reaction in the reforming process. The inverse process could adsorb part of the sensible heat, and store it in the produced syngas, thus improving the reforming efficiency of the fuel.

3.3. Major species profile

From the numerical result, the major species profile along the axial direction of the burner was shown in Fig. 5 for an inlet air flow rate of 5 L/min and an equivalence ratio of 1.5. The very high chemical reaction rate occurred within a small region, smaller than 0.01 m. After this violent combustion zone, the mole fraction of those major species changed slowly within the reforming zone. When the mole ratio of CO_2/CH_4 was 1, the mole fraction of CO_2 first decreased and then increased, indicating that CO_2 was consumed as a reactant at first and then generated as a reaction product in the downstream. As Fig. 5 shows, the mole fraction of H_2 increases more slowly, with CO_2. The reforming process of the mixture of CO_2 and CH_4 was different from that of the partial oxidation reforming of CH_4.

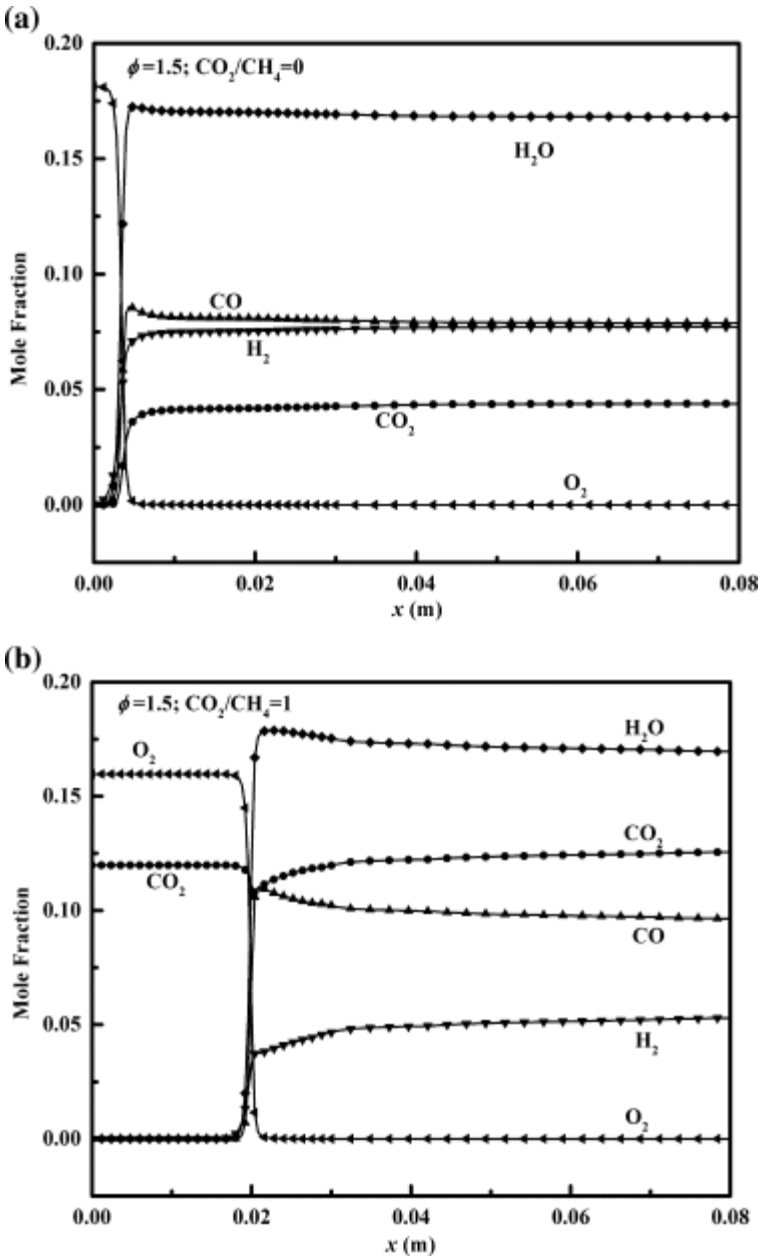

Fig. 5. Distribution of gas composition (mole fraction) along the axis direction of the burner.

3.4. Net reaction rate of CO_2

Based on the numerical simulation, the net reaction rates of CO_2 for various ratios of CO_2/CH_4 were shown in Fig. 6, for an inlet air flow rate of 5 L/min and an equivalence ratio of 1.5. It was found that the maximum net reaction rate of CO_2 decreased with increasing CO_2/CH_4 ratio. When the CO_2/CH_4 ratio was 1, part of the net reaction rate of CO_2 was negative, meaning that CO_2 initially participated in the reactions as a reactant rather than a product. During the initial stage of reaction, due to the large amount of heat provided from the porous media, the reforming reaction of CH_4 and CO_2 occurred before the partial oxidation of methane. According to the profile of the net reaction rate of CO_2 for a CO_2/CH_4 ratio of 1, the violent reaction region could be divided into three zones: preheating zone, CO_2-consuming

zone and CO_2 generation zone. In the preheating zone, the inlet premixed gases were preheated by the porous media and some pre-reactions occurred. In the CO_2-consuming zone, the reforming reaction of CH_4 and CO_2 was dominant: $CH_4 + CO_2 \rightarrow 2CO + 2H_2$. In the CO_2 generation zone, the partial oxidation reforming reaction of methane and the combustion reaction were the two main reactions: $CH_4 + 1/2O_2 \rightarrow CO + 2H_2$; $CH_4 + 2O_2 \rightarrow CO_2 + 2H_2O$. In addition, the WGS reaction was also an important reaction in the reforming zone, and the injection of CO_2 in the fuel also promoted the inverse WGS reaction.

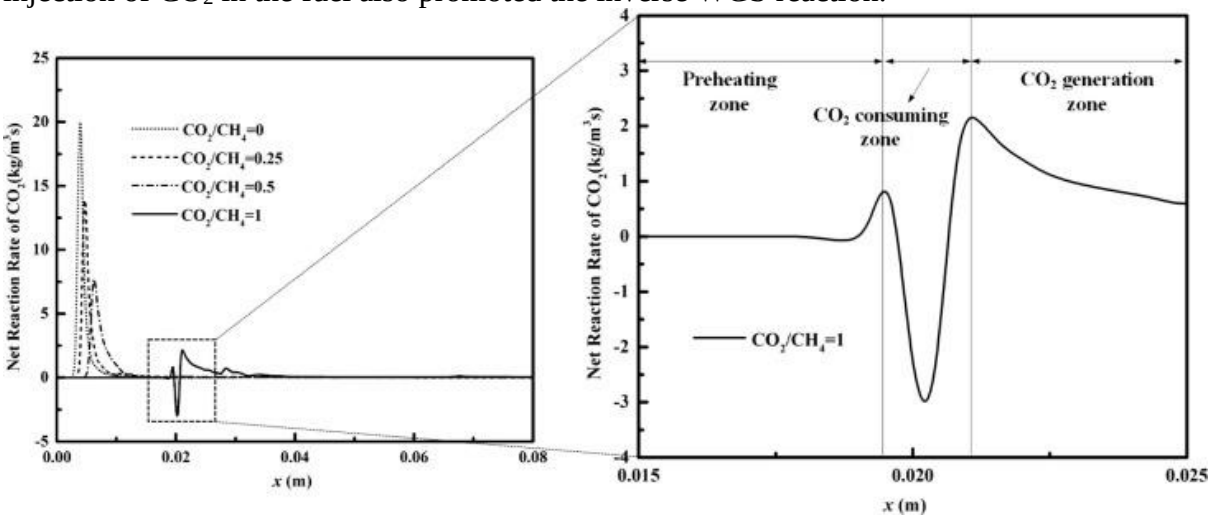

Fig. 6. The net reaction rate of CO_2 at inlet air flow rate of 5 L/min and equivalence ratio of 1.5.

4. Conclusions

A two-layer porous media burner was utilized for syngas production from fuel-rich combustion of CO_2/CH_4 mixtures with no catalyst. The experimental results showed that for an inlet air flow rate of 5 L/min and an equivalence ratio of 1.5, the reforming efficiency of fuel could be increased from 39.1% to 45.3% as the ratio of CO_2/CH_4 ratio increased from 0 to 1. The net emission for CO_2 can be reduced as a certain amount of CO_2, a typical component for many biomass-derived gases, was injected in the methane. A two-dimensional elementary reaction model was developed based on the experimental setup, with numerical results of the temperature distribution and major products matching well with the experimental results. The major species profile and the net reaction rate of CO_2 along the axis direction of the burner were simulated by the model. The violent chemical reaction occurred within a small region. For a CO_2/CH_4 ratio of 1, it could be divided into three zones: preheating zone, CO_2-consuming zone and CO_2 generation zone. From the numerical results, for a CO_2/CH_4 ratio of 1, CO_2 was consumed as a reactant first and then generated as a reaction product. The injection of CO_2 inhibited the WGS reaction, recovering part of the sensible heat to the syngas, and increased the reforming efficiency of fuel.

Acknowledgements

The authors acknowledge the Project 51576112 supported by National Natural Science Foundation of China, Project 2014CB249201 supported by the National Basic Research Program of China (973 Program), and Beijing Higher Education Young Elite Teacher Project and Tsinghua University 221 Fundamental Research Program. Meng Ni acknowledge the Project (PolyU 152173/15E) by The Hong Kong Polytechnic University (G-YBJN).

References

[1] O.V. Shapovalova, Y.N. Chun, M.S. Lim, V.M. Shmelev, V.S. Arutyunov

Syngas and hydrogen production from biogas in volumetric (3D) matrix reformers
Int J Hydrogen Energy, 37 (2012), pp. 14040-14046

[2] H.J. Van, Y. Membrez, O. Bucheli

Biogas as a fuel source for SOFC co-generators
J Power Sources, 127 (2004), pp. 300-312

[3] A. Galvagno, V. Chiodo, F. Urbani, F. Freni

Biogas as hydrogen source for fuel cell applications
Int J Hydrogen Energy, 38 (2013), pp. 3913-3920

[4] R. Horng, M. Lai, W. Lai

The assessment of reformation in a porous medium-catalyst hybrid reformer under excess enthalpy condition
Int J Hydrogen Energy, 37 (2012), pp. 14114-14123

[5] B. Hua, M. Li, Y. Sun, Y. Zhang, N. Yan, J. Chen, *et al.*

Biogas to syngas: flexible on-cell micro-reformer and NiSn bimetallic nanoparticle implanted solid oxide fuel cells for efficient energy conversion

J Mater Chem A, 4 (2016), pp. 4603-4609

[6] H.J. Alves, J.C. Bley, R.R. Niklevicz, E.P. Frigo, M.S. Frigo, C.H. Coimbra-Araújo

Overview of hydrogen production technologies from biogas and the applications in fuel cells
Int J Hydrogen Energy, 38 (2013), pp. 5215-5225

[7] A.I. Tsyganok, T. Tsunoda, S. Hamakawa, K. Suzuki, K. Takehira, T. Hayakawa

Dry reforming of methane over catalysts derived from nickel-containing Mg–Al layered double hydroxides
J Catal, 213 (2003), pp. 191-203

[8] K. Takehira, T. Shishido, P. Wang, *et al.*

Autothermal reforming of CH_4 over supported Ni catalysts prepared from Mg–Al hydrotalcite-like anionic clay

J Catal, 221 (2004), pp. 43-54

[9] D. Pakhare, J. Spivey

A review of dry (CO_2) reforming of methane over noble metal catalysts
Chem Soc Rev, 43 (2014), pp. 7813-7837

[10] Q. Jing, H. Lou, L. Mo, X. Zheng

Comparative study between fluidized bed and fixed bed reactors in methane reforming with CO_2 and O_2 to produce syngas
Energy Convers Manage, 47 (2006), pp. 459-469

[11] A.M. O'Connor, J.R. Ross

The effect of O_2, addition on the carbon dioxide reforming of methane over Pt/ZrO_2, catalysts
Catal Today, 46 (1998), pp. 203-210

[12] M.K. Drayton, A.V. Saveliev, L.A. Kennedy, *et al.*

Syngas production using superadiabatic combustion of ultra-rich methane-air mixtures

Symp Combust, 1 (1998), pp. 1361-1367

[13] M.J. Dixon, I. Schoegl, C.B. Hull, *et al.*

Experimental and numerical conversion of liquid heptane to syngas through combustion in porous media

Combust Flame, 154 (2008), pp. 217-231

[14] H.S. Colin, M.L. Daniel, E.M. Liane, *et al.*

Conversion of wet ethanol to syngas via filtration combustion: an experimental and computational investigation

Proc Combust Inst, 33 (2011), pp. 3317-3324

[15] Z. Al-Hamamre, A. Al-Zoubi

The use of inert porous media based reactors for hydrogen production
Int J Hydrogen Energy, 35 (2010), pp. 1971-1986.

[16] H. Liu, S. Dong, B.W. Li, *et al.*

Parametric investigations of premixed methane–air combustion in two-section porous media by numerical simulation

Fuel, 89 (2010), pp. 1736-1742

[17] H. Pedersen-Mjaanes, L. Chan, E. Mastorakos

Hydrogen production from rich combustion in porous media
Int J Hydrogen Energy, 30 (2005), pp. 579-592

[18] Wang, H. Zeng, T. Cao, *et al.*

Start-up and operation characteristics of a flame fuel cell unit

Appl Energy, 178 (2016), pp. 415-421

[19] Y. Wang, H. Zeng, A. Banerjee, *et al.*

Elementary reaction modeling and experimental characterization on methane partial oxidation within catalyst enhanced porous media combustor

Energy Fuels, 30 (2016), pp. 7778-7785

[20] Z. Al-Hamamre, A. Al-Zoubi, D. Trimis

Numerical investigation of the partial oxidation process in porous media based reformer
Combust Theor Model, 14 (2010), p. 91

[21] W.M. Pitts, E. Braun, R.D. Peacock, *et al.*

Temperature uncertainties for bare-bead and aspirated thermocouple measurements in fire environments

ASTM Spec Tech Publ, 1427 (2002), pp. 3-15

[22] H. Pedersen-Mjaanes

Hydrogen production from rich combustion inside porous media
University of Cambridge, UK (2006)

[23] F. Mauss, N. Peters

Reduced kinetic mechanisms for premixed methane-air flames
N. Peters, B. Rogg (Eds.), Reduced kinetic mechanisms for applications in combustion systems, Springer, Berlin (1993), pp. 58-75